Urban Climate 39 (2021) 100937

Contents lists available at ScienceDirect

Urban Climate

journal homepage: www.elsevier.com/locate/uclim

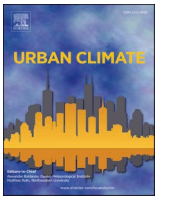

Observing the impact of urban morphology and building geometry on thermal environment by high spatial resolution thermal images

Jinxin Yang [a,*], Qian Shi [b,*], Massimo Menenti [c,d], Man Sing Wong [e], Zhifeng Wu [a], Qunshan Zhao [f], Sawaid Abbas [e], Yong Xu [a]

[a] School of Geography and Remote Sensing, Guangzhou University, Guangzhou 510006, China
[b] School of Geography and Planning, Sun Yat-sen University, Guangzhou 510275, China
[c] Faculty of Civil Engineering and Earth Sciences, Delft University of Technology, P. O. Box 5048, 2600 GA Delft, Netherlands
[d] State Key Laboratory of Remote Sensing Science, Institute of Remote Sensing and Digital Earth, Chinese Academy of Sciences, Beijing 100101, China
[e] Department of Land Surveying and Geo-Informatics, The Hong Kong Polytechnic University, Kowloon, Hong Kong
[f] Urban Big Data Centre, School of Social and Political Sciences, University of Glasgow, Glasgow G12 8RZ, UK

ARTICLE INFO

Keywords:
Urban morphology
Urban thermal environment
Urban surface temperature
High-resolution thermal imagery

ABSTRACT

Urban surface temperature is a very important variable in the observation and understanding of energy exchange. A comprehensive understanding of the urban thermal environment is of great significance towards the adaptability of urban areas to climate hazards. The heterogeneity of urban space increases the complexity of the urban surface temperature observations and the analyses of the energy exchange. To understand how the urban geometry affects the distribution of surface temperature, we used airborne thermal infrared remotely sensed images at very high spatial resolution (original spatial resolution is 0.2 m × 0.2 m after registration). We did this study in Hong Kong to analyze the effects of various geometric parameters on different facet surface temperatures (roof, road, wall and vegetation) in daytime and nighttime and in different seasons. Results show that the urban geometry has greater impacts on the road temperature than on building temperature, and the impact of the geometric parameters on road surface temperature changes with the time of the day and the season. The building height is a more effective driver of heat dissipation in daytime than nighttime for roof facets. A lower building density improves ground heat dissipation, while a higher building density improves heat dissipation by roof facets. Furthermore, the vegetation only limitedly affects the surface temperatures of facets that are lower than vegetation, but to an extent useful to mitigate urban temperature, which might be a feature relevant in urban design. This research can provide insights useful to city planners and policy makers to better understand the urban thermal environment and help design more livable and healthy cities in the near future.

1. Introduction

The increasing number of urban residents, the proliferation of megacities, and the rapid expansion of *peri* urban areas are one of the

* Corresponding author.
E-mail addresses: Yangjx11@gzhu.edu.cn (J. Yang), shixi5@mail.sysu.edu.cn (Q. Shi), m.menenti@tudelft.nl (M. Menenti), lswong@polyu.edu.hk (M.S. Wong), zfwu@gzhu.edu.cn (Z. Wu), Qunshan.Zhao@glasgow.ac.uk (Q. Zhao), xu1129@gzhu.edu.cn (Y. Xu).

https://doi.org/10.1016/j.uclim.2021.100937
Received 26 March 2021; Received in revised form 12 June 2021; Accepted 22 July 2021
Available online 27 July 2021

most challenging transformation of the 21st century (Wentz et al., 2018). In 2018, 55% of world population lives in urban areas, with the projection to 68% in 2050 (United Nations, 2018). Specifically, urbanization increases both the density and the height of the urban space. The modification of urban surfaces with new urban geometry and man-made materials make the urban surface temperature significantly different from the rural areas (Oke, 1988). Buildings and vegetation block and scatter the solar radiation, which enhances thermal heterogeneity because of the heterogeneous shaded and sunlit patterns (Wang et al., 2020; Yang et al., 2020). Buildings also increase the overall urban surface area, i.e. the total area per unit horizontal area, which means more solar radiation is absorbed in urban areas. With less vegetation coverage in cities, it results in less energy consumed for evaporation and transpiration to cool down the urban space and surrounding atmosphere (Oke, 1988; Oke et al., 1999). All these factors affect the energy exchange in the urban areas and create a unique urban climate environment.

The urban surface temperature is an important variable in the observation and understanding of urban thermal environment under different urban design conditions (Voogt and Oke, 2003; Weng, 2009). Urban geometry and materials have significant effects on the spatial distribution of the urban surface temperature at micro and *meso* scales and these effects were analyzed in multiple previous studies, mostly using numerical models (Ali-Toudert and Mayer, 2006; Franck et al., 2013; Goldberg et al., 2013; Henon et al., 2009; Hilland and Voogt, 2020; Hou and Estoque, 2020; Kanda et al., 2005; Kastendeuch and Najjar, 2009; Kondo et al., 2001; Krayenhoff and Voogt, 2007; Li et al., 2011; Logan et al., 2020; Morrison et al., 2018; Yang and Li, 2013; Yang and Li, 2015). At the micro-scale, those studies investigated how urban geometry and materials affect the urban surface temperature, e.g. street, roof, vegetation, and wall surface temperatures, based on simplified 3D urban canyon models (Wang, 2014) Kondo et al., 2001; Kanda et al., 2005; Krayenhoff and Voogt, 2007; Kastendeuch and Najjar, 2009; Yang and Li, 2013). At the *meso* scale, the interactions between urban land cover and the urban surface temperature have also been studied by using thermal infrared radiometric data collected by space- and airborne imaging radiometers, that can provide real observations of the urban surface (Chen et al., 2006; Weng et al., 2004; Yuan and Bauer, 2007). Peng et al. (2020) analyzed the correlation between urban surface temperature and its drivers with land cover and normalized building/vegetation difference indices. The results showed that the normalized built-up index explained to a large extent the observed warming of urban areas. The geometry effect of built-up areas on the urban surface temperature has been also studied to understand the drivers of observed surface urban heat island by using satellite thermal infrared data and the building geometric data (Huang and Wang, 2019; Yu et al., 2019). In general, the low spatial resolution of satellite thermal images does not hinder the acquisition of useful observations, but makes it impossible to accurately understand how urban geometries and surface characteristics influence the urban land surface temperature distribution at micro-scale, particularly when the information provided by low-resolution satellite thermal images is the average of mixed pixels in high-resolution satellite images.

The urban surface is heterogeneous in both the horizontal and the vertical dimension because of the complex materials and geometric characteristics. The temperatures of building wall, building roof, road pavement, and urban vegetation contribute differently to the urban energy exchange and climate. However, the complex heterogeneity and geometry of urban surfaces make it very difficult to observe and interpret surface temperatures when using low or moderate spatial resolution thermal images. The variability of surface temperature results in a complex urban surface energy exchange and leads to anisotropy of urban exitance, which includes the longwave emittance by the urban objects and the emittance by the atmosphere reflected by the built-up space (Lagouarde et al., 2012; Lagouarde and Irvine, 2008; Wang et al., 2018). Space-borne observing systems designed to measure radiance at multiple view angles are needed to obtain the component temperatures of urban facets (Menenti et al., 2001). This complexity is neglected by many current studies, though it affects both the acquisition of remote sensing data and their interpretation towards a better understanding of urban climate (Hu and Brunsell, 2013; Zhan et al., 2012).

Considering different facets have diverse effects on the urban energy exchanges and urban microclimate, understanding the drivers of the variability in facet temperature has been necessary for urban planners and architects, because it is important to understand the potential influence from urban design to urban microclimate environment (Hilland and Voogt, 2020; Wetherley et al., 2018; Yaghoobian et al., 2010). Zhao et al. (2015) analyzed the main drivers of rooftop surface temperature using high resolution thermal remotely sensed data (7m/pixel) acquired by an airborne imaging radiometer and results showed that rooftop surface temperature is closely related to the material attributes and rooftop geometry. Yang and Li (2015) analyzed the effect of building geometry and albedo on the street surface temperature by numerical experiments and results showed that there was a clear relationship between the street surface temperature and the Sky View Factor (SVF). Wetherley et al. (2018) analyzed the effects of urban geometry and materials on vegetation surface temperature with high resolution thermal images and results showed that building density had multiple effects on tree and turfgrass surface temperature.

Different urban objects may have different thermal response because of their location and the geometric characteristics of the surroundings. For example, the green roof surface is ineffective to improve thermal comfort at ground level, while trees at street level are effective in cooling pedestrian areas (Ng et al., 2012). In general, the main driver of thermal heterogeneity is urban geometry in the vicinity of each facet, so that the facet surface temperature may vary in a very large range because of the complex urban geometric characteristics. Moreover, the urban geometry may cause different effects on component surface temperatures in daytime and nighttime, leading to a different thermal anisotropy in daytime and nighttime (Lagouarde et al., 2012; Lagouarde et al., 2010).

Detailed understanding on how the urban geometry determines the facet temperatures and thermal heterogeneity within facets of the same type, is important for research on urban climate and urban planning. Although this has been studied with microclimate numerical simulation models, the models have been simplified for both land surface processes and the details in 3D building/vegetation structures to reduce computational load. Low-resolution remotely sensed satellite thermal imagery cannot provide the detailed component surface temperatures. To address this research gap, numerous researchers attempted to use high spatial resolution thermal images to observe component temperatures and study energy exchanges in urban areas (Lagouarde et al., 2004; Xu et al., 2008), e.g. the MODIS/ASTER Airborne Simulator (MASTER) imagery for urban heat island research (Zhao and Wentz, 2016). This research

showed that airborne high spatial resolution images can capture the thermal heterogeneity of urban components and the images are important data sources to understand urban thermal environment.

The overarching goal of this research is to understand the thermal behavior of different types of urban facets and help urban planners and architects to better understand how to alleviate urban heat load and create more livable and healthier urban environment based on experiment results. High resolution airborne thermal images provide details about the urban facet temperatures to investigate how the geometry affects the variability of surface temperature within each facet type in daytime and nighttime.

2. Data and study areas

Airborne high spatial resolution (HR) thermal data observed over the urban area of Kowloon (Fig. 1) were used in this study. The thermal camera of FLIR T650sc was set on a helicopter and the flight height was 610 m. The spectral coverage of the camera is from 7.5 to 13μm. The field of view is 25° and the large field of view (FOV) helps obtain wall information. The original spatial resolution of the HR data is 0.5 m × 0.5 m. The HR thermal images used in this study were obtained in daytime and nighttime on Oct 24, 2017 (autumn) and Jan 14, 2018 (winter), respectively. On Oct 24, 2017, the HR thermal data were obtained from about 11:30 (first stripe) to 12:20 (last stripe) in daytime and from 20:00 to 20:47 during nighttime. On Jan 14, 2018, the HR thermal data were obtained from 13:32 to 14:40 in daytime and from 20:30 to 21:30 during nighttime. The designed flight lines were same for the four flights (Fig. 2). There are multiple flight lines and directions. Each stripe overlaps partly with adjacent stripes. Thus, some facets can be observed along 3stripes from 4 directions, and some other facets along 2 stripes from 4 directions, i.e. wall facets may be observed from multiple directions. The bias due to observation geometry cannot be completely avoided, thus there might be some residual impact on the images collected during the four flights (Fig. 3). The thermal images observed by thermal camera were processed using the FLIR ResearchIR Max software (https://www.flir.cn/products/flir-thermal-studio-suite/) to derive the urban surface temperature. From the meteorological stations of Hong Kong Observatory (HKO) and King's Park (KP), the weather conditions at observation times are presented in Table 1. Results showed that the cloud cover on both days was rather low in daytime (14% and 11%). The mean wind speed in daytime on Oct 24 2017 and Jan 14 2018 was the same (11.5 m/s). Conversely, in nighttime, the mean wind speed on Oct 24 2017 and Jan 14 2018 was different.

To calculate the urban surface temperature, the atmospheric temperature and relative humidity observed at the Hong Kong Observatory were input into FLIR ResearchIR Max to correct for the atmospheric effects. The spectral library of impervious urban materials (Kotthaus et al., 2014) contains 74 samples of impervious surfaces and was adopted in this study to obtain the material emissivity in urban areas for HR thermal images. The majority of building materials in the study area are cement, concrete and bricks, and the majority of road materials are asphalt, cement, or concrete. Thus, we used the mean material emissivity of cement, concrete and bricks to estimate the emissivity of roof and wall facets and mean material emissivity of asphalt, cement, and concrete to estimate

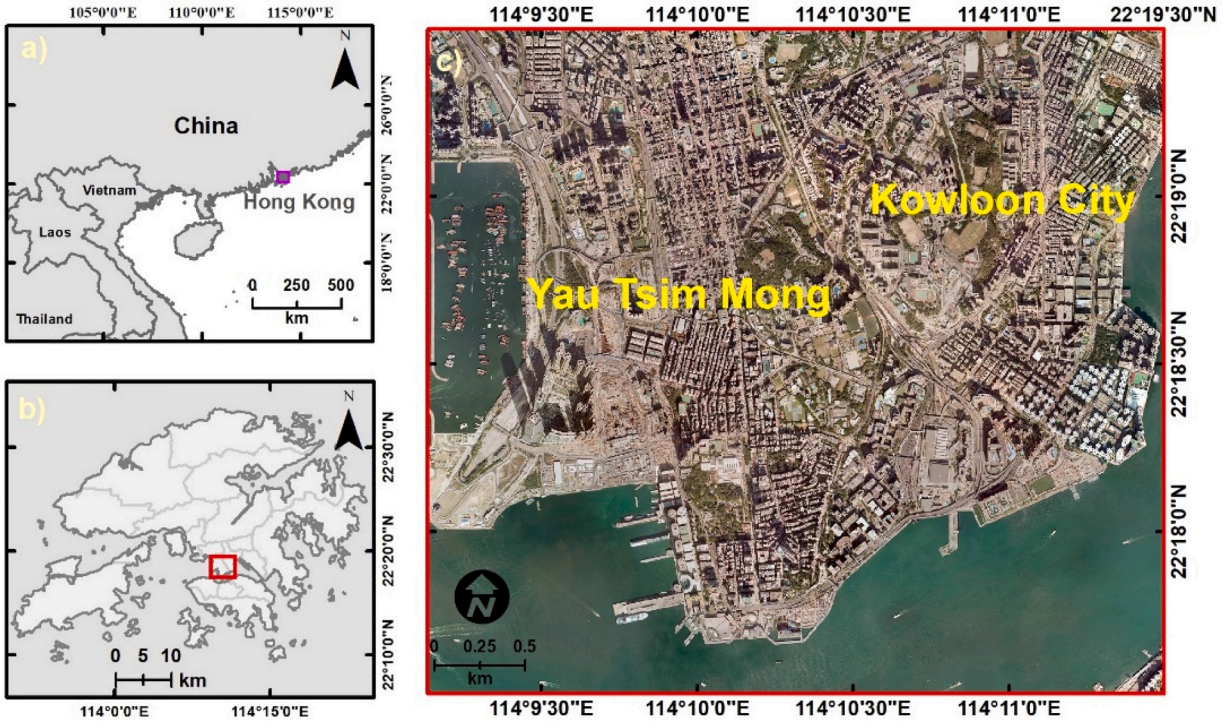

Fig. 1. Study area.

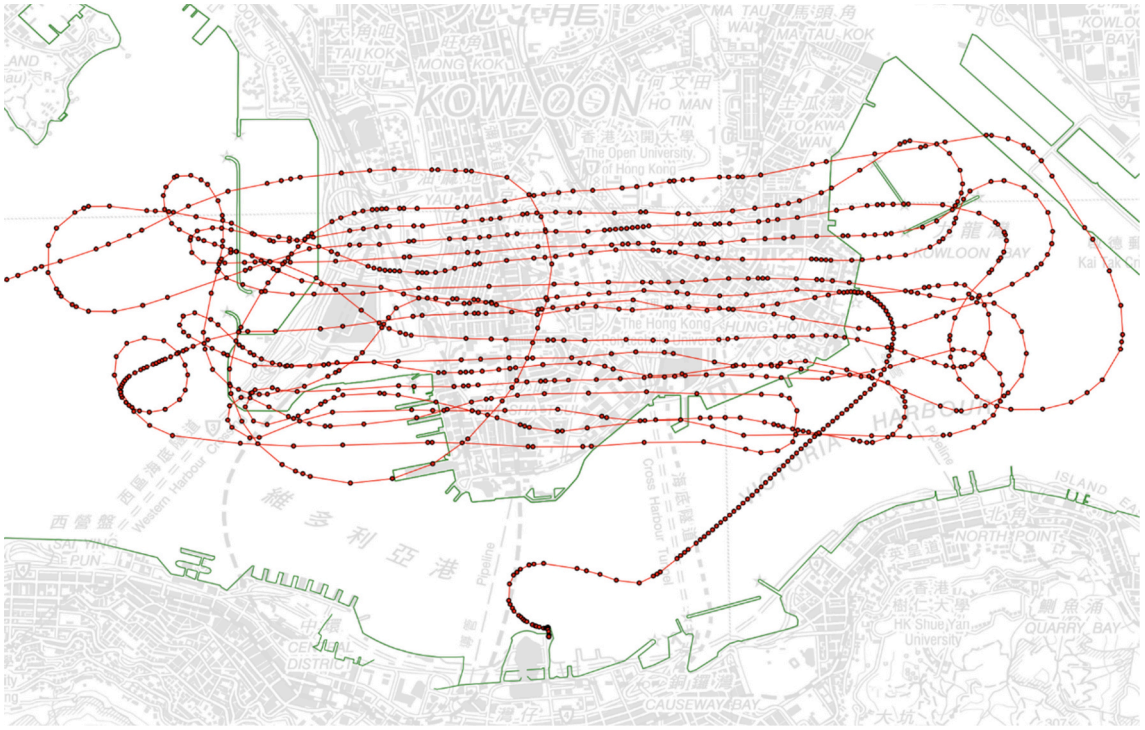

Fig. 2. Fight lines in the flight experiments.

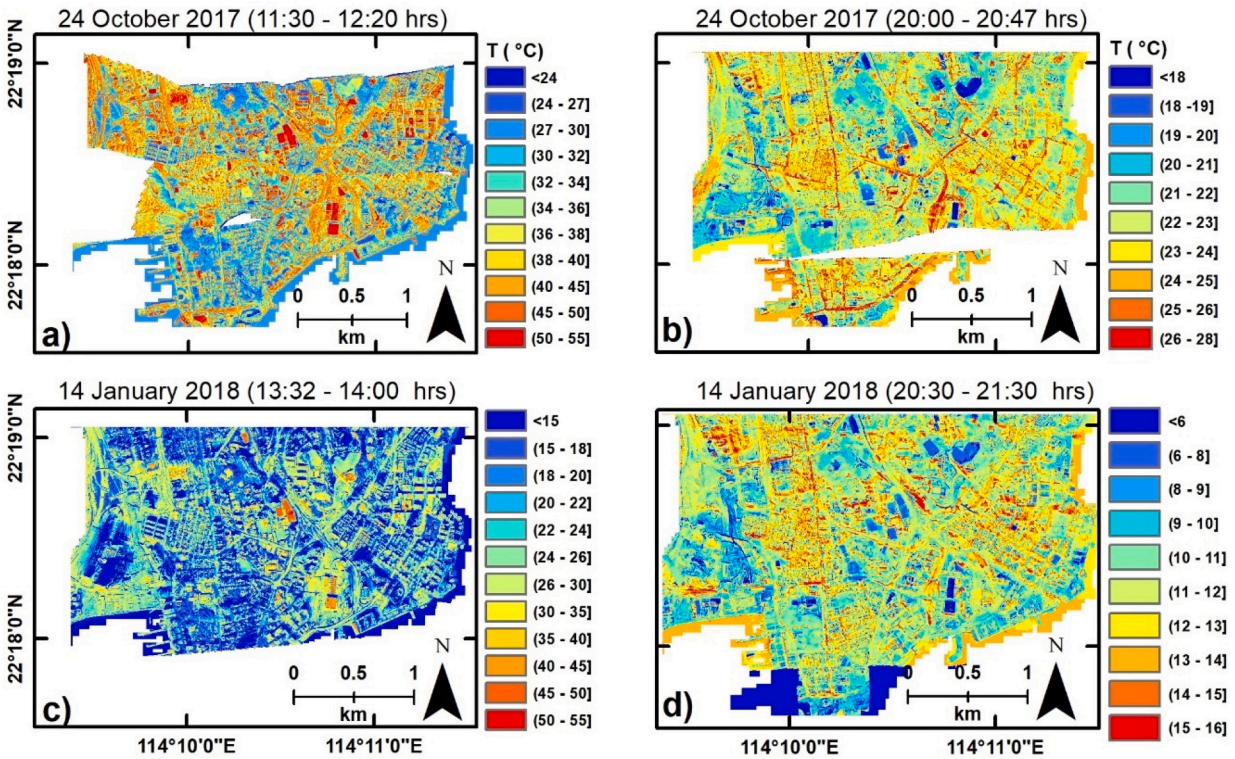

Fig. 3. High spatial resolution airborne thermal images (1 m).

Table 1
Weather conditions at observation time.

	2017/10/24			2018/1/14		
	12:00	20:00	21:00	14:00	20:00	21:00
Cloud coverage (HKO)	14% (daily data)			11% (daily data)		
Temperature (HKO) °C	26.8	24.4	24.1	16.3	14.2	14.2
Humidity (HKO) %	53	64	68	60	78	79
Wind speed (KP, 10-min average) m/s	11.5	9.4	10.1	11.5	No data	6.5
Wind direction (KP, 10-min average)	134	113	126	121	No data	128
Rainfall	0	0	0	0	0	0

the emissivity of road facets. The final emissivity of roof and wall is 0.932 and the emissivity of road is 0.945 in this analysis. ASTER Spectral Library 2.0 (Baldridge et al., 2009) was used to estimate the material emissivity of vegetation, which was 0.973.

Besides the HR thermal images, we obtained the DSM data, HR multispectral image, building shapefile and road shapefile data from the HK Planning Department and these data are strictly registered and ortho-rectificated. The co-registration accuracy of HR thermal images and HR optical image is better than 1 pixel. More information about the data in Fig. 3can be referred to Yang et al. (2016). To match the HR thermal images with the Digital Surface Model (DSM), the HR thermal images were aggregated to 1 m × 1 m. The airborne HR multispectral image of Kowloon obtained in 2015 (resolution 0.5 m × 0.5 m) (Fig. 1) was used to extract accurate vegetation cover. The building shapefile data and DSM data with 1 m spatial resolution were used to calculate the building density, shadows, sky view factor and building height (Fig. 4) (Yang et al., 2021). The DSM data is from territory-wide airborne LiDAR data obtained from December 2010 to January 2011 and the horizontal and vertical accuracies are 0.3m and 0.1 m respectively (Lai et al., 2012). The road information was extracted from road shapefile. Changes in the urban area of Kowloon have been very small after 2010 thus these data can be used together.

3. Method

The methodology framework of this study is shown in Fig. 5. The building shapefile and road shapefile provide information on road and building facets assuming nadir viewing. The FOV of the airborne thermal camera is rather large and captures off-nadir information on observed targets. On the other hand, roof and wall facets observed by the thermal camera may not exactly fit with the building shapefile. To solve this problem, we have manually extracted the target components, i.e. the roof, road, wall and vegetation facets from the HR thermal images (Fig. 3). Fig. 6 shows an example of the extracted roof, road and wall facets from the HR thermal images. The roof and road segments extracted from the building shapefile and land use classification were intersected with the HR thermal data to

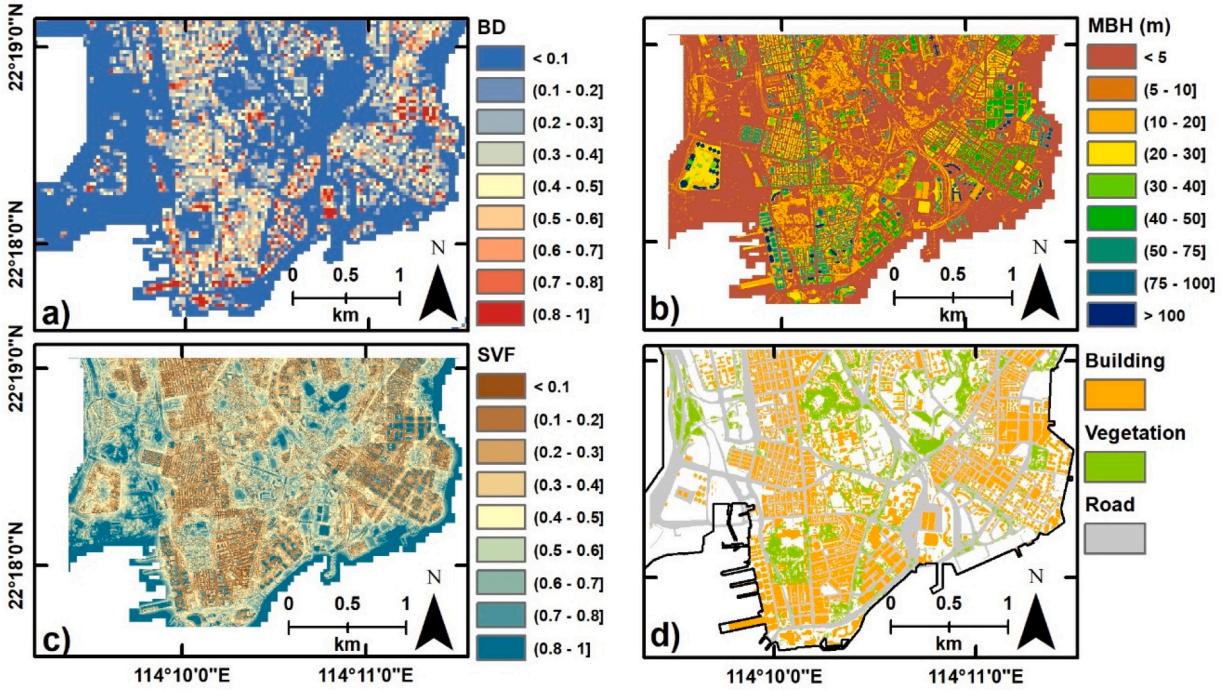

Fig. 4. Building geometric data. a) building density; b) building height; c) SVF; and d) land cover map (building roof, vegetation and road).

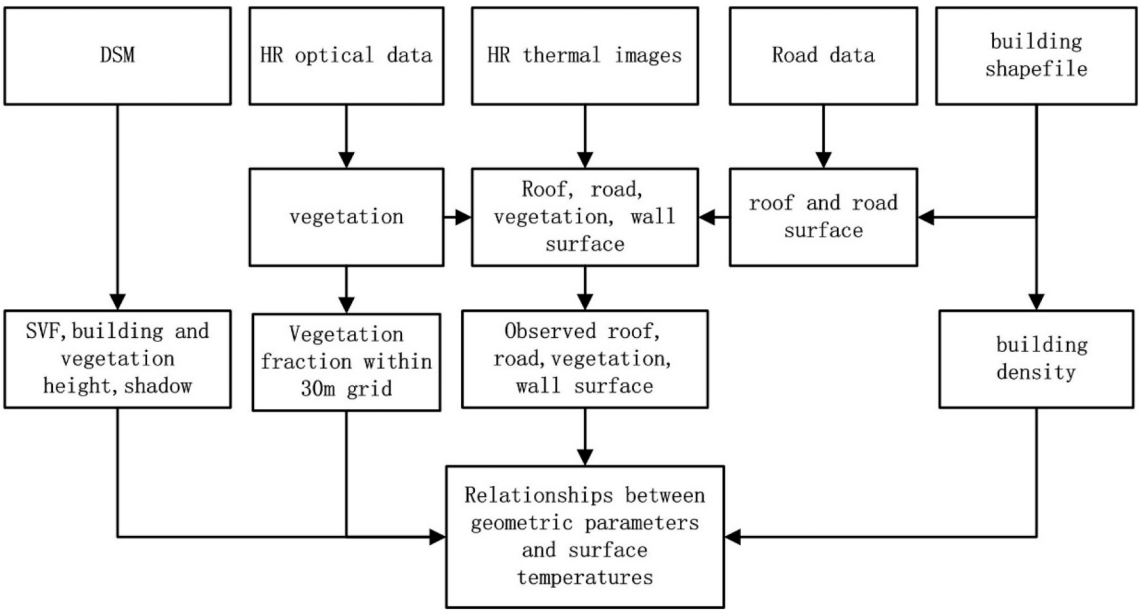

Fig. 5. Methodology framework.

determine the actually observed roof and road facets. Only the roof facets observed from nadir or near-nadir in the HR thermal data were used to analyze the effects of urban geometry on the roof and road facet surface temperature. The vegetation facets were extracted from the HR visible airborne data manually and applied as a reference to determine the actually observed vegetation facets in the HR thermal images.

In this study, multiple source data were used. The HR optical data are 0.5 m, which means the pixel size is 0.5 m × 0.5 m. The HR thermal data after processing and DSM are 1 m. Neither the building density or the fractional vegetation cover could be retrieved for each pixel at these resolutions and had to be retrieved by gridding all the data sets to a common grid size. The fractional vegetation cover and building density were respectively retrieved as the fraction of vegetation and building pixels within each grid. As regards the grid size, a grid of 30 m × 30 m was finally adopted, since the data would be easier to combine with L8 OLI and TIRS data, which are so commonly used in urban studies. Thus, the HR visible image was orthorectified and was applied to estimate the vegetation fraction within each 30 m × 30 m grid. For wall facets, we only considered the parts that we could capture. The facet surface temperatures of road (T_g), roof (T_r), wall (T_w) and vegetation (T_v) were analyzed to understand the effects of urban geometry on land surface temperature.

To calculate the surface temperature of each components, we took into account the emissivity of the extracted component facets based on Stefan-Boltzmann law:

$$T_s = T_b \Big/ \sqrt{4\varepsilon} \tag{1}$$

In Eq. (1), T_s is the facet surface temperature, T_b is the brightness temperature after atmospheric correction obtained from the FLIR

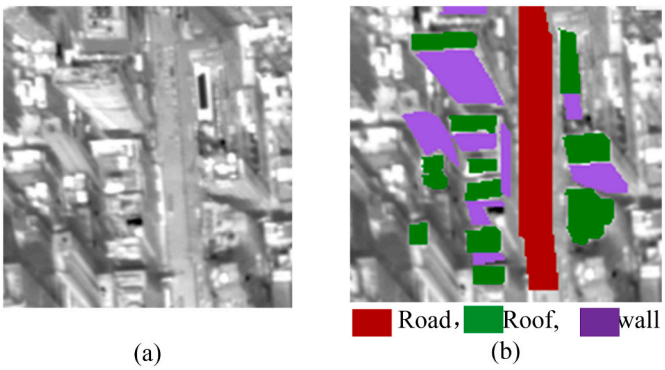

Fig. 6. Example for the extraction of roof, road and wall from thermal images manually. (a) thermal images; (b) extracted roof, road and wall surface.

reprocessing software (ResearchIR Max), ε is the material emissivity of component facets.

The building density, building height, SVF and vegetation height were calculated from Digital Surface Model data (DSM) at 1 m × 1 m spatial resolution and the building shapefile. We calculated the building density within each 30 m × 30 m grid by calculating the building roof areas within each grid with the same as vegetation fraction. The SVF is calculated from DSM data and the calculation method was described in detail by Yang and Li (2015). The building height was also extracted by combining the building shapefile with the DSM data. The relation between building height and the roof temperature was analyzed. The SVF at 1 m spatial resolution was used to analyze the relation between SVF and component temperatures including roof, road and wall facets. Considering that the amount of data is large and affected by noise, we calculated the mean surface temperature of road and roof facets within each 0.1 SVF interval and 0.1 building density interval to determine the relationship between the surface temperature of road and roof and SVF/building density at a significant level of 0.05. The sunlit facets receive more solar radiation and shadow facets receive no direct solar irradiance, thus the building density, building height and SVF may have different effects on sunlit and shadow facets. The sunlit and shadow facets were separated by calculating shadows based on urban geometry. The shadow distribution was calculated from the DSM data combined with the solar angles at the time of acquisition of the HR thermal images by using the *hillshade* tool in ArcGIS. The analysis of daytime data was done separately for shadow and non-shadow facets.

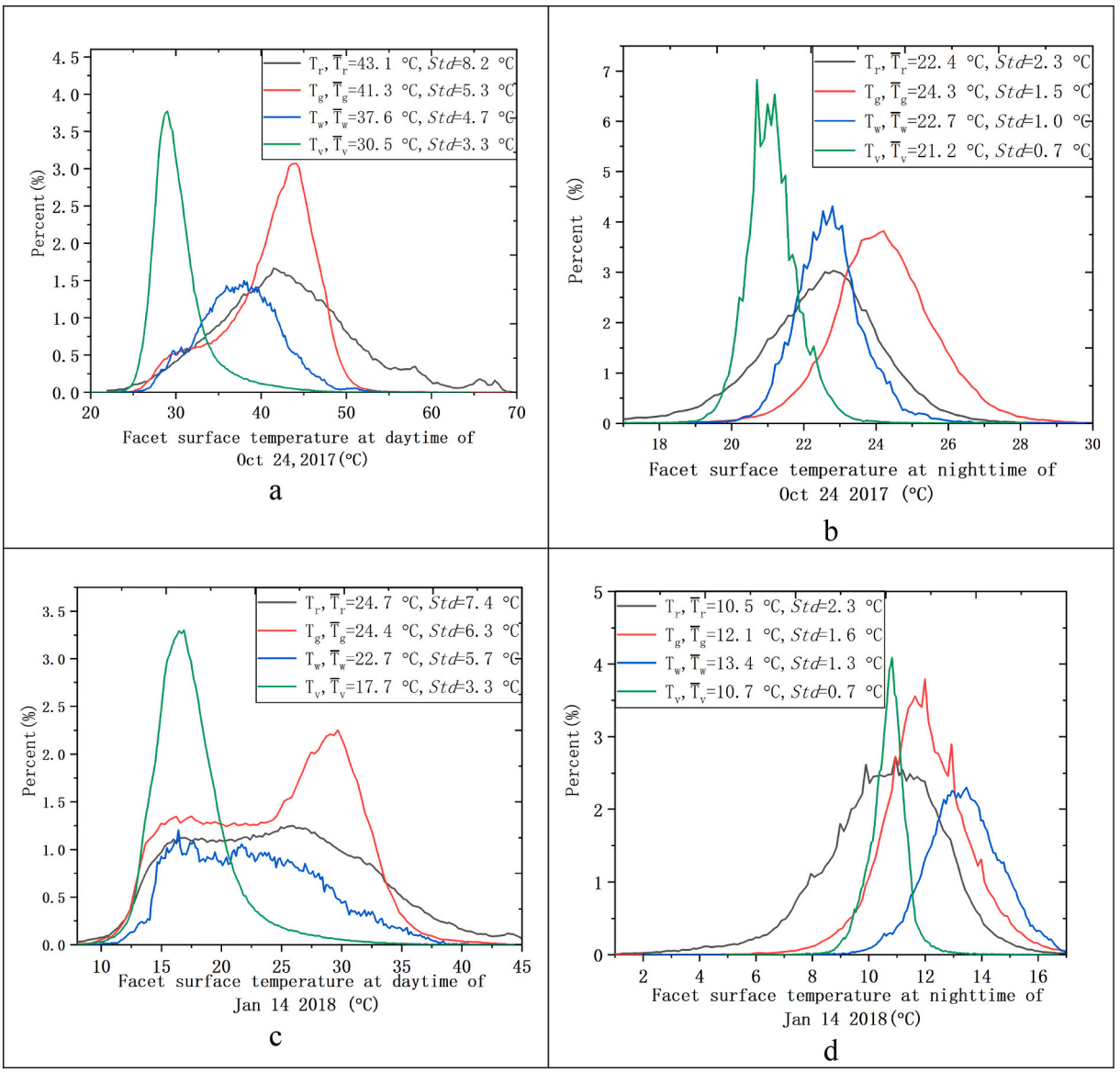

Fig. 7. HR thermal data and distributions of road, roof, vegetation and wall surface temperatures: a, Daytime of Oct 24 2017; b, nighttime of Oct 24 2017; c, daytime of Jan 14 2018; d, nighttime of Jan 14 2018. (T_r, T_g, T_w and T_v are roof, ground/road, wall and vegetation surface temperature respectively,$\overline{T_r}$, $\overline{T_g}$, $\overline{T_w}$ and $\overline{T_v}$ are mean surface temperatures of roof, ground/road, wall and vegetation, *Std* is Standard Deviation)

4. Results

4.1. Observed variability of facet surface temperatures

HR thermal data can capture the variability of facet surface temperature within and between different facet types. This variability can be large even within the same type of facets (Fig. 7), e.g. the variability of roof temperature is higher than road temperature. Fig. 7 showed the temperature histograms of roof, road, wall and vegetation to show the variability of component facet temperatures. This is indicated by the standard deviations of daytime roof surface temperature (T_r), i.e. 8.2 °C on Oct 24, 2017 and 7.4 °C on Jan 14, 2018 against 5.3 °C and 6.3 °C for T_g. Road facets receive less solar irradiance compared with roof facets because of the blocking effects by the surrounding built-up components. Roof facets receive more solar irradiance and this enhances the thermal heterogeneity within roof facets, i.e. it results in higher thermal heterogeneity of roof facets than road facets. During daytime, mean value of T_r is higher than that of T_g and the difference between T_r and T_g changes with the season. In autumn, the difference between mean values of T_r and T_g is 1.9 °C, while this value is rather small (0.3 °C) in the winter. The reason is that the solar irradiance on Oct 24, 2017 (autumn) was higher than Jan 14, 2018 (winter). Higher solar irradiance enhances the surface temperature differences caused by materials and geometry. During nighttime, T_g was higher than T_r, but the difference between T_r and T_g did not change much with the season. This is because the main driver of thermal environment at nighttime is the building geometry which does not change with season. T_w (Fig. 7) was lower than T_r and T_g in daytime but higher than T_r in nighttime. The standard deviations of T_w in daytime were 4.7 °C on Oct 24, 2017 and 5.7 °C on Jan 14, 2018, i.e. lower than T_r. In daytime, the wall facets receive less direct solar irradiance than roof and road. Thus, T_w in daytime is lower than T_r and T_g. During nighttime, radiative exchanges are characterized by diffuse atmosphere longwave irradiance onto wall facets, while exitance from opposite wall and ground facets can reach wall facets. When the SVF of a facet is very small, the radiation emitted by the facet will be absorbed by surrounding facets and then reflected and re-emitted to ground. Thus, low SVF limits the radiative losses from the urban canopy. This increases the energy absorbed by wall facets, with Tw being higher than Tr in nighttime.

Generally, the vegetation facets have relatively a smaller variability in surface temperature than road and roof facets. In daytime, the vegetation surface temperature is much lower than the surface temperatures of road and buildings, e.g. the difference between mean values of T_r and T_v was about 13.0 °C on Oct 24, 2017 and 7 °C on Jan 14, 2018 (Fig. 7). The differences between mean values of T_g and T_v in daytime were about 11.3 °C on Oct 24 2017 and 6.7 °C on Jan 14 2018. This indicates that vegetation cover may contribute significantly to reduce urban surface temperature. In nighttime, the difference between mean values of T_v and T_g was 3.1°C on Oct 24, 2017 and 1.4 °C on Jan 14, 2018. However. The difference between T_v and T_r is not obvious at nighttime in winter (Jan 14, 2018) (Fig. 7).

Fig. 7 shows that in the observed area the frequency distributions of the surface temperatures vary significantly across facet types. As expected all facets reach higher temperatures in daytime, but road facets reach extremely high temperatures, i.e. up to 70 °C, while vegetation is only slightly warmer in daytime, thus documenting the cooling effect of transpiration. The range in observed temperatures is much wider in daytime for all facets, particularly for road facets, thus showing how daytime irradiance amplifies the facet thermal response to radiative and convective cooling. The information on the distribution of facet temperatures and differences in the mean facet temperature, is very relevant to understand the thermal response to radiative forcing in a concise way. The differences in facet surface temperatures are caused by geometry and material compositions. Fig. 7 shows that the HR thermal images can capture such subtle details in the response of urban space to radiative and convective forcing. Both urban materials and geometry affect the

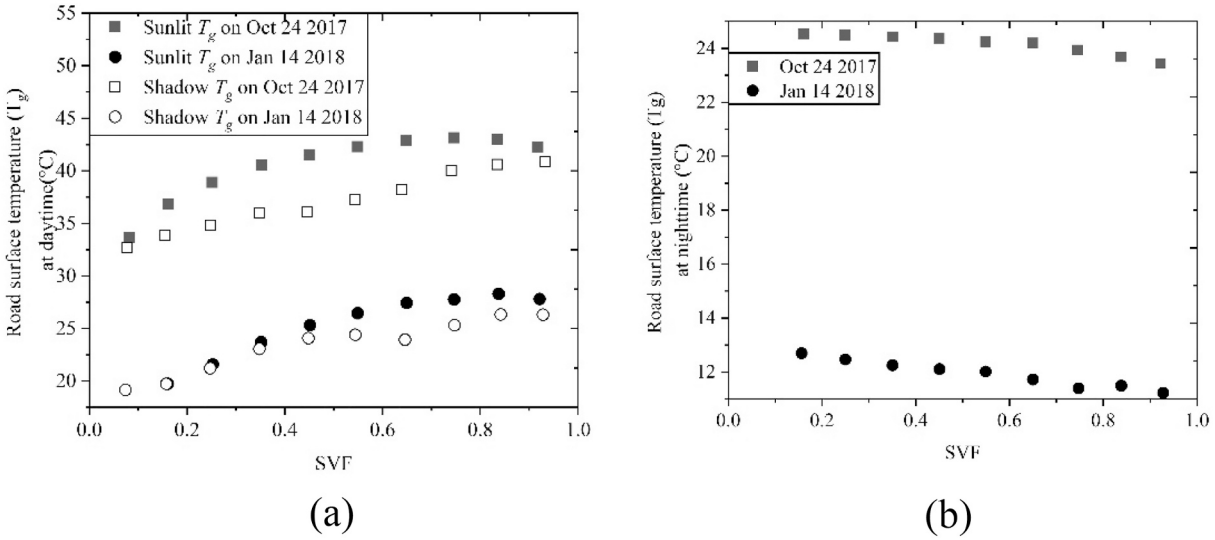

Fig. 8. Relationship between T_g and SVF: (a) daytime sunlit road; (b) nighttime.

surface temperature and its variability. For different facets and meteorological conditions, the dominant drivers of surface temperature are different. The relative magnitude of impact of urban materials vs. urban geometry needs to be characterized towards a better understanding of urban climate. In the following sections we will analyze how the geometric parameters drive the variability of facet temperatures and we will attempt to identify the dominant drivers of the thermal heterogeneity of the built-up space based on the entire areas covered by the data in Fig. 3.

4.2. Relationship between component temperatures and SVF

The T_g is clearly related to SVF under both sunlit and shadow conditions (Fig. 8a). The HR retrievals of urban surface temperature were first binned at 0.1 SVF intervals, then averaged to obtain the T_g applied to regress the relationship with SVF. Results showed that the relationship between sunlit T_g and SVF was logarithmic (Table 2). Sunlit T_g increased with SVF, while the rate of increase of T_g decreased with SVF. Contrariwise, the relationship between shadow T_g and SVF was not logarithmic: on Oct 24, 2017 was nearly linear, while on Jan 14, 2018 it was logarithmic, but with a break-point at about SVF = 0.6. This means there are different driving factors of T_g under different conditions. The range in T_g of a sunlit road surface between SVF = 0.1 and SVF = 1 reached 9.5 °C on Oct 24, 2017 and 8.1 °C on Jan 14, 2018, while for a shadowed road surface, the range in T_g was 8.2 °C on Oct 24, 2017 and 7.2 °C on Jan 14, 2018. It should be noted that the occurrence of shadowed road facets is highly dependent on the time of acquisition of HR thermal images. When the SVF is close to 0 or close to 1, the surface temperature differences between sunlit and shadowed road surface are very small. When SVF is close to 0, the road surface is likely surrounded by very high buildings, the sunlit road surface may only be sunlit at the time of image acquisition. Thus, the sunlit T_g is close to shadowed T_g. When SVF is close to 1.0, the road surface is in a wide open surrounding. Thus, road facets may be shadowed just for a short time, if at all, and this may occur just at the time of image acquisition. This makes the shadowed T_g similar to the sunlit T_g. Thus, the building shadow has a significant impact on road or ground surface temperature for intermediate SVF values, from 0.5 to 0.65.

In nighttime, T_g decreased slightly with SVF and the range in T_g was 1.1 °C on Oct 24, 2017 and 1.4 °C on Jan 14, 2018 ((Fig. 8 (b)). A smaller SVF indicates trapping of longwave exitance within the urban canopy. Thus, road facets with higher SVF cool down sooner than facets with smaller SVF. The relations between SVF and T_g in nighttime were also different: quadratic polynomial on Oct 24, 2014 and linear on Jan 14, 2018.

The relation between T_r and SVF in daytime and nighttime was evaluated in a similar way (Fig. 9). The sunlit T_r increased almost linearly with SVF (Fig. 9a and Table 2), while the shadow T_r varied slightly with SVF, but no relationship could be established. The range in T_r of a sunlit roof surface in daytime was 5.8 °C on Oct 24, 2017 and 4.9 °C on Jan 14, 2018, which is much smaller than the range in T_g over the same SVF range. This indicates that SVF has a larger effect on T_g than on roof surface temperature. The shadow T_r decreased with SVF on Oct 24, 2017 and increased with SVF on Jan 142,018. The reason may be the observation time: on Oct 24, 2017 the HR data were acquired between 11:30 and 12:30 and slightly later, i.e. between 13:30 and 14:30 on Jan 14th 2018. It was more likely to have roof facets being sunlit for part of the time on Jan 14th 2018 and thus the roof surface temperature is higher with larger SVF. In nighttime T_r is almost constant with SVF and just decreases very slightly (Fig. 9b), i.e. less than 1 °C.

In daytime, T_w increases with SVF (Fig. 10(a)) and the relation between T_w and SVF was logarithmic (Table 2). Irradiance on vertical facets increases with increasing SVF, thus higher SVF results in higher T_w in daytime. On the other hand, the range in T_w was about 2 °C on Oct 24, 2017 and about 6 °C on Jan 14, 2018 (Fig. 10(a)), i.e. much smaller than in T_g and T_r during daytime, as shown above. In nighttime, the range in T_w is also very small, although the ranges were slightly different on Oct 24, 2017 and Jan 14, 2018. In the nighttime of Oct 24, 2017, T_w decreased with SVF, while it increased with SVF on Jan 14, 2014 (Fig. 10(b)). In general, a higher SVF improves cooling during the night, thus the wall, roof and road surface temperatures should decrease with increasing SVF. On the other hand, irradiance does also increase with increasing SVF, so the observed range in facet surface temperature is driven by the balance of two opposite drivers: increasing radiative load and increasing convective cooling. In addition, clouds may reduce radiative cooling in nighttime, an effect likely to be larger on vertical wall facets where clear-sky radiative cooling increases significantly with increasing SVF.

The difference in facet temperatures between daytime and nighttime was also very sensitive to SVF (Fig. 11). The difference in T_r increased with SVF linearly (Fig. 11(a) and Table 3). The difference in T_g between daytime and nighttime also increased with SVF but logarithmically, and stabilized at SVF ≈ 0.7 (Fig. 11 (b) and Table 3). The difference in T_r between daytime and nighttime was higher

Table 2
Estimated relationships between the surface temperatures of horizontal facets (y) and SVF (x).

Daytime	2017/10/24	2018/01/14	Nighttime	2017/10/24	2018/01/14
Sunlit road	$y = 3.9139\ln(x) + 44.082$ $R^2 = 0.9533$	$y = 5.1537\ln(x) + 29.131$ $R^2 = 0.9792$	Road	$y = -2.0562x^2 + 0.8564x + 24.416$ $R^2 = 0.99$	$y = -1.8636x + 12.943$ $R^2 = 0.9765$
Shadow road	$y = 9.5051x + 32.361$ $R^2 = 0.9789$	$y = 3.0436\ln(x) + 26.17$ $R^2 = 0.9387$			
Sunlit Roof	$y = 6.0006x + 39.469$ $R^2 = 0.9228$	$y = 6.2321x + 21.61$ $R^2 = 0.9647$	Roof	$y = -0.12\ln(x) + 22.44$ $R^2 = 0.7925$	$y = -0.161\ln(x) + 10.322$ $R^2 = 0.8648$
Shadow roof	$y = -2.3152x + 37.707$ $R^2 = 0.365$	$y = 2.8017x + 21.69$ $R^2 = 0.868$			
Wall	$y = 2.4394\ln(x) + 40.037$ $R^2 = 0.807$	$y = 5.0877\ln(x) + 27.7$ $R^2 = 0.906$	Wall	$y = -0.8162x + 22.6$ $R^2 = 0.354$	$y = 0.3977x + 13.189$ $R^2 = 0.4864$

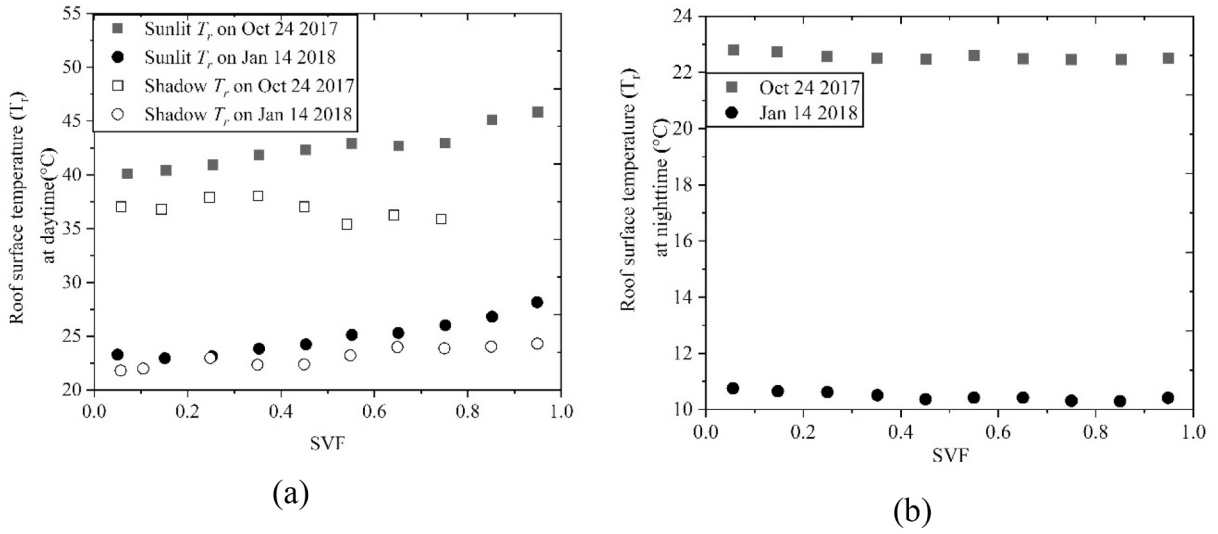

Fig. 9. Relationship between T_r and SVF: (a) daytime; (b) nighttime.

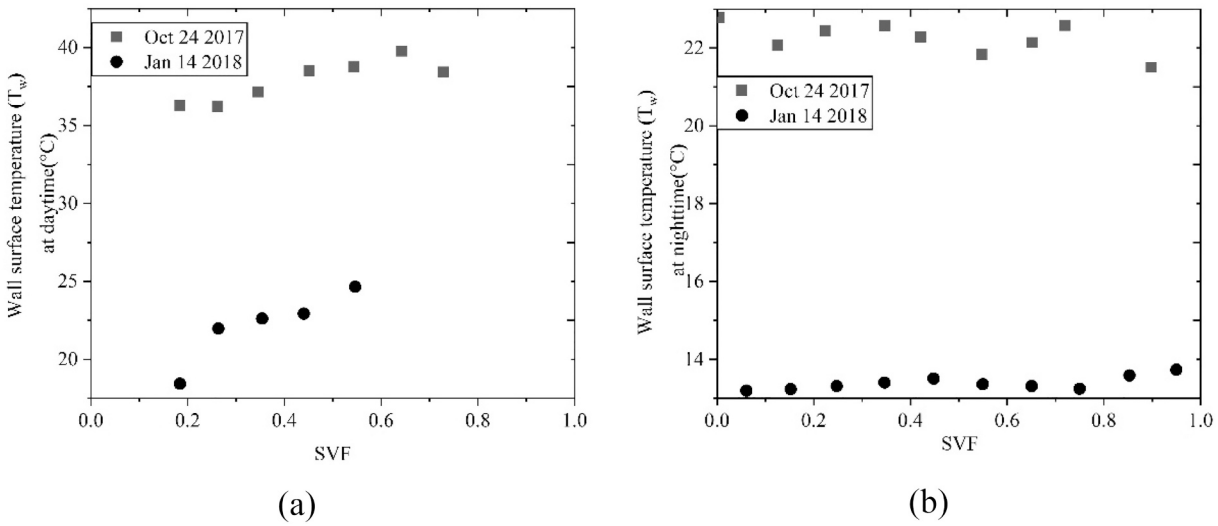

Fig. 10. Wall surface temperature vs. SVF: (a) daytime; (b) nighttime.

than in T_g. In daytime, T_r was higher than T_g because irradiance onto a roof facet is higher than on a road facet. At nighttime, T_r was lower than T_g. This means that roof facets are more efficient in dissipating heat than road facets during nighttime. The heat dissipation is the total energy lost by the urban canopy to the atmospheric boundary layer by radiative and convective exchanges. Higher heat dissipation means more efficient cooling.

4.3. Building height

The relation between T_r and building height has also been studied (Fig. 12). Results showed that the T_r of sunlit roof decreased with increasing building height (Fig. 12(a)). The T_r of shadow roof facets also decreased with increasing building height, but the sensitivity is lower than sunlit roof facets. The range in T_r over the range in building height reached 10 °C for a sunlit roof facet. In nighttime, T_r decreased very slightly with building height on Oct 24th 2017 and appeared insensitive to building height on Jan 14th 2018 (Fig. 12 (a)), as shown by the very low correlation coefficients between T_r and building height, i.e. only 0.0053 (Table 4). This means that the building height only affects sunlit T_r in daytime, while the building height is not the dominant driver of surface temperature for a shadowed roof surface in daytime and in nighttime. It should be noted that changes in urban geometric parameters are correlated. For example, higher buildings lead to larger frontal area, which increases convective exchanges, and larger SVF for roof facets, which increases irradiance onto roof facets but increases the longwave radiation dissipation. Summarizing, the increase in building height

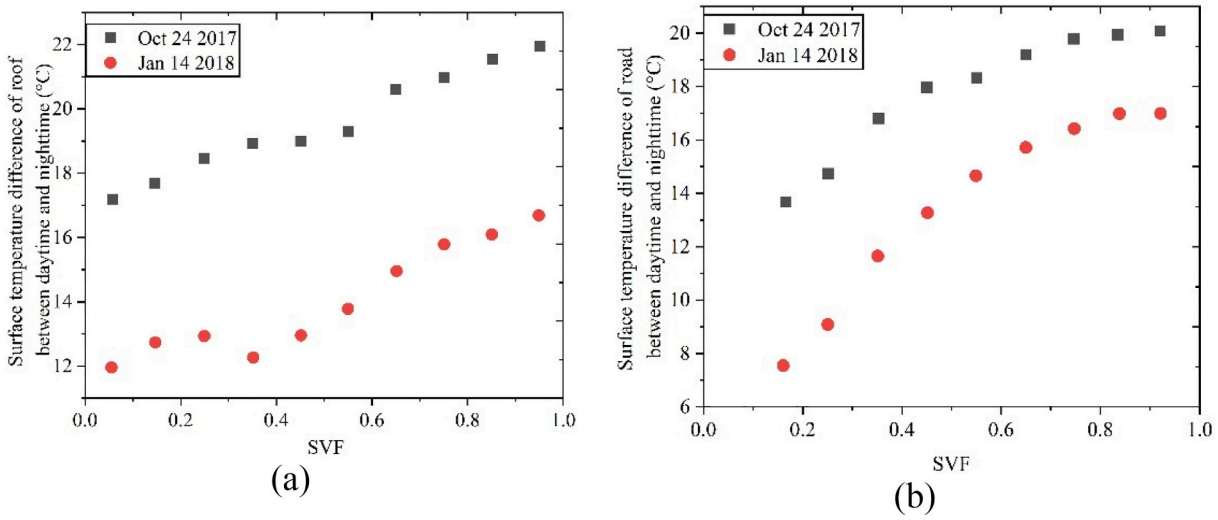

Fig. 11. Difference in component temperatures between daytime and nighttime vs. SVF: (a) roof; (b) road.

Table 3
Estimated relationships between the daytime - nighttime difference in surface temperature and SVF.

	Roof	Road
2017/10/24	$y = 5.3231x + 16.883$ $R^2 = 0.977$	$y = 3.9981\ln(x) + 20.755$ $R^2 = 0.9848$
2018/01/14	$y = 5.4081x + 11.304$ $R^2 = 0.9006$	$y = 5.9053\ln(x) + 17.941$ $R^2 = 0.989$

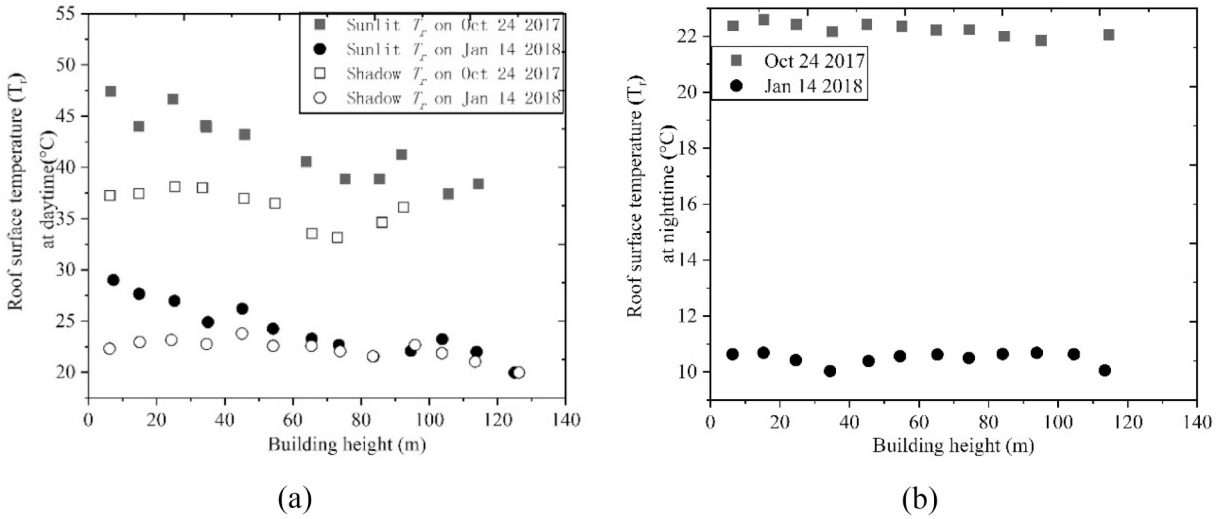

Fig. 12. Roof surface temperature vs. building height: (a) daytime; (b) nighttime.

Table 4
Regression equations between roof facet surface temperatures and building height.

Daytime	2017/10/24	2018/01/14	Nighttime	2017/10/24	2018/01/14
Sunlit Roof	$y = -0.0843x + 46.946$ $R^2 = 0.851$	$y = -0.0651x + 28.351$ $R^2 = 0.872$	Roof	$y = -0.0051x + 22.526$ $R^2 = 0.6566$	$y = -0.0005x + 10.516$ $R^2 = 0.0053$
Shadow roof	$y = -0.0317x + 37.914$ $R^2 = 0.3546$	$y = -0.0188x + 23.474$ $R^2 = 0.5521$			

decreased the sunlit T_r in daytime (Fig. 12(a)). The dependence of radiative and convective exchanges on building geometry is more complex in the case of shadows and in nighttime, thus suggesting a weaker dependence of T_r on building height in these cases (Fig. 12 (b) and Table 4).

The difference in T_r between daytime and nighttime decreased with building height (Fig. 13 and Table 5). This was to be expected, since T_r in daytime decreased with building height (see Fig. 12), while it decreased very slightly in nighttime.

Building height has complex effects on T_w, but it was very difficult to extract the temperature of all wall facets and, moreover, the distribution of T_w changes with building height. Thus, the relation between T_w and building height cannot be evaluated as done with roof temperature.

4.4. Building density

T_r had no clear relationship with building density in both daytime and nighttime (Fig. 14(a) and (b)). The regression analysis on T_r and building density showed that there is only a very slight increasing trend in daytime (Table 6). In daytime both sunlit and shadowed T_g decreased with increasing building density, but the impact of building density on sunlit road facets was larger than on shadowed road (Fig. 15 (a) and Table 6). During nighttime, T_g does not increase with building density (Fig. 15(b) and Table 6). Similarly, the building density has no obvious effects on T_w (Fig. 16 and Table 6), possibly because of the difficulty in extracting a large number of wall facets. Summarizing, the building density only affects T_g in daytime, but has no clear effects on other facet temperatures.

Day - night difference in road temperature (Fig. 17 (b) and Table 7) decreased with increasing building density, while it increased for T_r (Fig. 17(a)). Higher building density reduces both convective cooling of and radiative load on road facets, thus explaining the decreasing trend in Fig. 17(b). This means that a higher building density reduces the cooling rate of a road surface. The day-night difference in T_r increases with increasing building density (Fig. 17(a)). This means the increase of building density helps to increase the cooling rate of T_r.

4.5. Vegetation

Vegetation temperature decreased slightly with increasing vegetation height and fractional abundance (Fig. 18 and Fig. 19). This means that the vegetation height increase helps to reduce the vegetation surface temperature. Changes in T_r were negligible when fractional abundance of vegetation was smaller than 0.5, while T_r decreased with vegetation fractional abundance when vegetation fraction was higher than 0.5. After we checked the DSM data, we found that the vegetation height is higher than roof height where vegetation fraction is larger than 0.6, e.g. low or medium buildings surrounded by high trees. Thus, the relative height of building and vegetation may be a main reason for the effects of vegetation on T_r. T_g on Jan 14, 2018 decreased with the fractional abundance of vegetation, possibly because of increasing shadows. Conversely, on Oct 24, 2017 the data were acquired at about 12:00, i.e. with minimal shadows and T_g did not change significantly with the fractional abundance of vegetation. T_w did not change significantly with fractional abundance on Oct 24, 2017 and decreased on Jan 142,018 because the shadow effects on Jan 14 might have been heavier (Fig. 19 and Table 8). These results indicate that vegetation affects the surrounding surface temperature in multiple ways and the height of vegetation relative to the surrounding surface has significant effects as regards the cooling effects of vegetation.

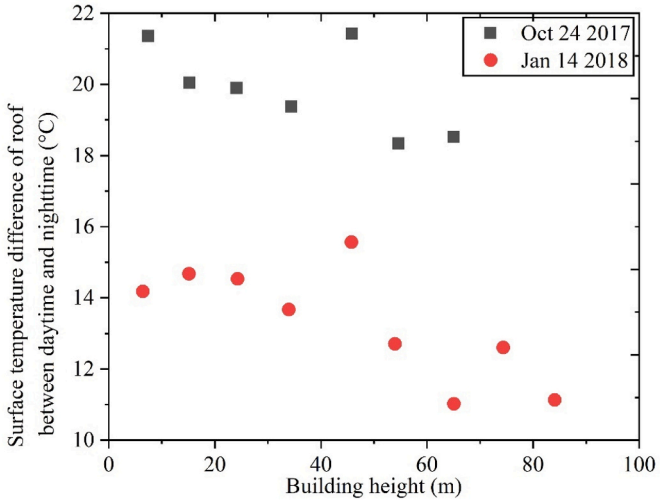

Fig. 13. Difference between daytime and night in roof temperature vs. building height.

Table 5
Regression equations between road / roof day-night temperature difference and building height.

Date	Roof
2017/10/24	$y = -0.0366x + 21.139$ $R^2 = 0.3974$
2018/01/14	$y = -0.0447x + 15.343$ $R^2 = 0.5742$

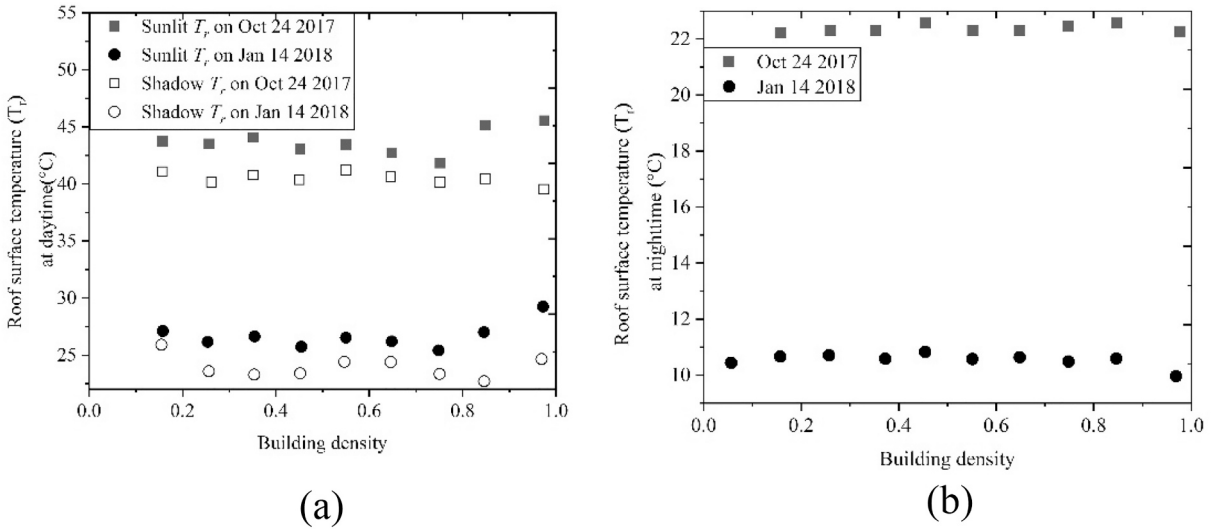

Fig. 14. Roof surface temperature vs. building density: (a). daytime; (b). nighttime.

Table 6
Regression equations between road / roof daytime - nighttime temperatures and building density.

	2017/10/24 daytime	2018/01/14 daytime	2017/10/24 nighttime	2018/01/14 nighttime
Sunlit road	$y = -5.2151x + 41.316$ $R^2 = 0.9224$	$y = -7.5808x + 25.291$ $R^2 = 0.8198$	$y = -1.1143x + 24.943$ $R^2 = 0.5924$	$y = -0.54x + 12.833$ $R^2 = 0.293$
Shadow road	$y = -4.623x + 34.481$ $R^2 = 0.310$	$y = -6.8721x + 23.428$ $R^2 = 0.7957$		
Sunlit Roof	$y = 1.2809x + 42.949$ $R^2 = 0.0936$	$y = 1.597x + 25.783$ $R^2 = 0.1548$	$y = 0.144x + 22.28$ $R^2 = 0.0832$	$y = -0.6105x + 10.896$ $R^2 = 0.4682$
Shadow roof	$y = -1.0623x + 41.073$ $R^2 = 0.326$	$y = -1.0444x + 24.538$ $R^2 = 0.0884$		
Wall	$y = -1.035x + 37.675$ $R^2 = 0.1007$	$y = -0.1073x + 22.875$ $R^2 = 0.0165$	$y = 0.2354x + 22.724$ $R^2 = 0.0153$	$y = 0.5347x + 13.149$ $R^2 = 0.2597$

5. Discussion

The geometry effects on urban surface temperature have been studied by numerous researchers based on different data source (Harman et al., 2004; Hilland and Voogt, 2020; Huang and Wang, 2019; Yang and Li, 2015; Zhao et al., 2015). Such studies help to understand the impact of urban design on urban climate. In general, microclimate models apply a simplified description of urban land surface processes, e.g. turbulent heat transfer, and the models cannot necessarily capture urban processes in a comprehensive and exact way. On the other hand, satellite data cannot provide detailed information on component facets, because of the relatively low spatial resolution. To fill this research gap, we analyzed the urban geometry effects on facet temperature using HR thermal infrared data.

Yang and Li (2015) studied the impacts of SVF on street surface temperature by numerical experiments and the results showed that street surface temperature changes logarithmically with SVF in summer and linearly in winter. In this study, we separately analyzed the sunlit and shadow road facets in autumn (2017 Oct 24th) and winter (2018 Jan 14th). Results showed that the dependence on geometric parameters of sunlit T_g in autumn and winter is close to logarithmic, while it is linear in autumn and logarithmic in winter for shadowed road facets. In nighttime, the SVF had different impacts on T_g than in daytime.

The geometric parameters have more significant effects on T_g than on T_r. Some geometric parameters have no obvious impacts on

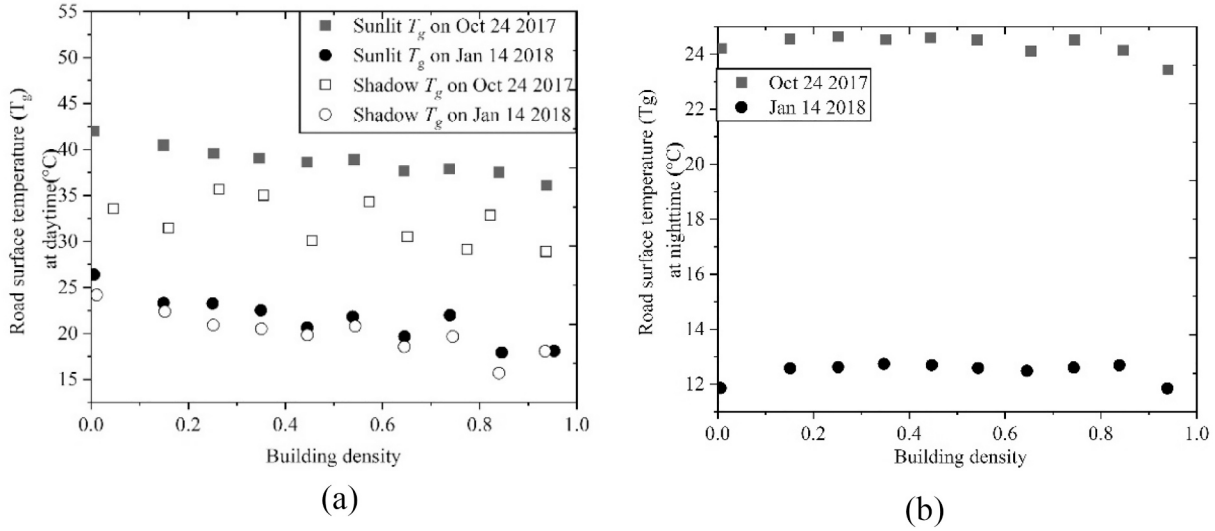

Fig. 15. T_g vs. building density: (a). daytime; (b). nighttime.

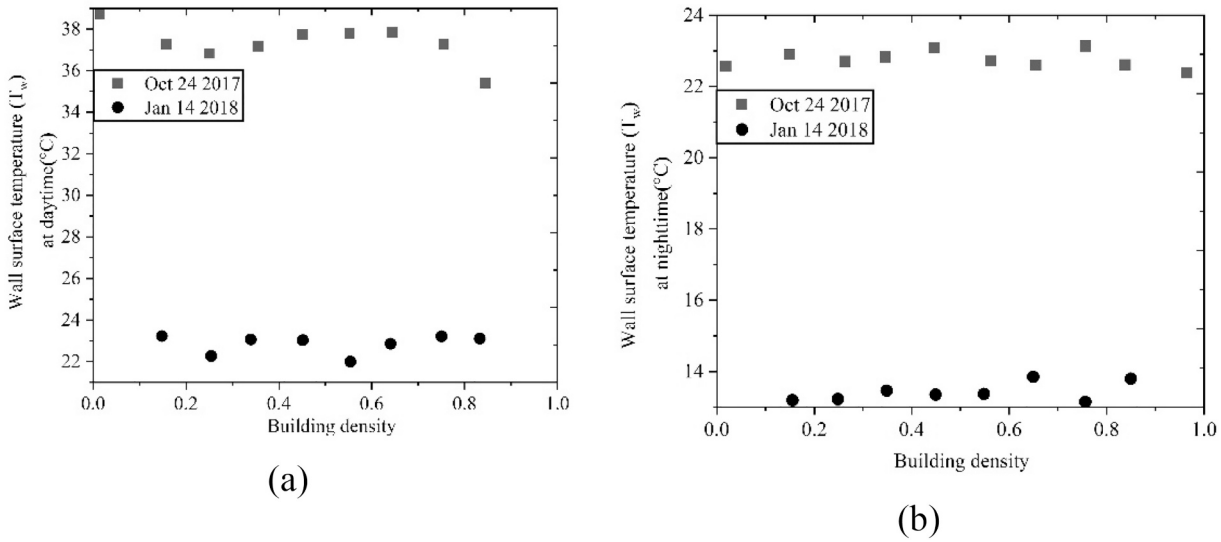

Fig. 16. Wall surface temperature vs. building density: (a) daytime; (b) nighttime.

roof surface temperature under some conditions. In this study, the geometry has more significant effects on the roof surface temperature in daytime than nighttime. In nighttime, the roof surface temperature changes very slightly with geometry parameters. This means the geometry has very limited effects on nighttime roof surface temperature. In daytime, the effects of building height on roof surface temperature were more significant than building density. These results are similar to the conclusions from Zhao et al. (2015). In Zhao et al. (2015), results showed also that the dominant factors for roof surface temperature are different in daytime and nighttime and geometric parameters have more significant effects on roof surface temperature in daytime than nighttime. The vegetation effects on roof surface temperature also change with the vegetation height. When vegetation is higher than the buildings, the roof surface temperature decreased with increasing fractional abundance of vegetation, as expected. Additionally, the distance between vegetation and rooftop also affects the vegetation effects, although here we did not consider it.

Wall facets are an important component of the built-up space (Hilland and Voogt, 2020). Wall surface temperature is also complex because of wall geometry and of the impact of adjacent buildings and vegetation. Hilland and Voogt (2020) analyzed the effect of facet geometry on the wall surface temperature and showed that sub-facet geometry has significant effects on wall surface temperature distribution because of the shadow effects. In this study, we could retrieve the surface temperature of a limited number of wall facets observable with the HR data, thus our results on wall surface temperature may be biased. Based on the dataset we obtained, the wall surface temperature does not change significantly with building density. The change of wall surface temperature with vegetation

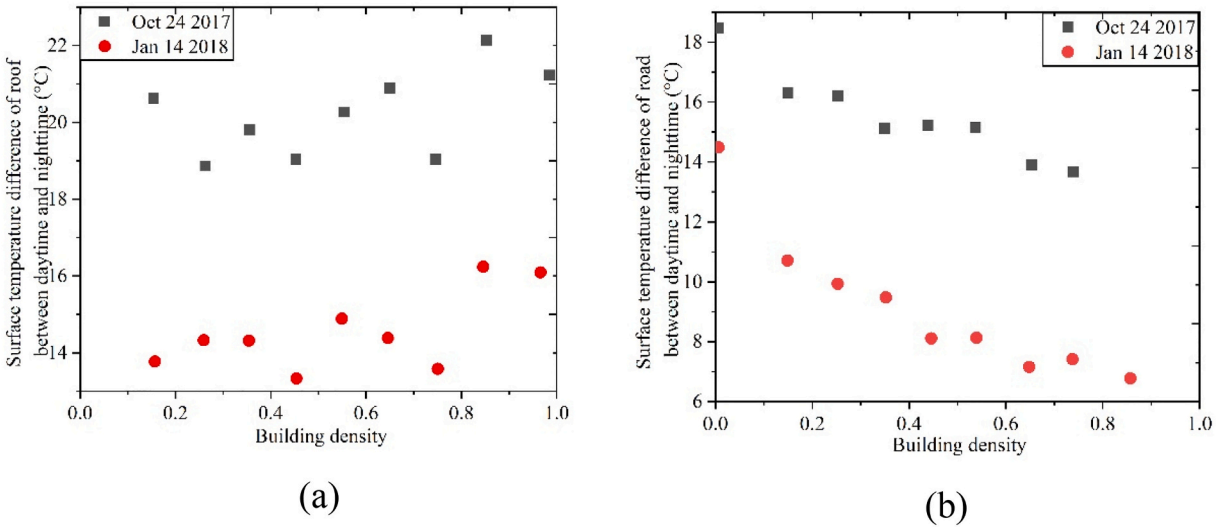

Fig. 17. Day - night temperature difference vs. building density: (a). roof; (b). road.

Table 7
Regression equations between road / roof day –night temperature difference and building density.

	Roof	Road
2017/10/24	$y = 2.0773x + 19.05$ $R^2 = 0.2625$	$y = -0.837\ln(x) + 14.399$ $R^2 = 0.8073$
2018/01/14	$y = 2.4572x + 13.186$ $R^2 = 0.4224$	$y = -1.52\ln(x) + 7.1418$ $R^2 = 0.9438$

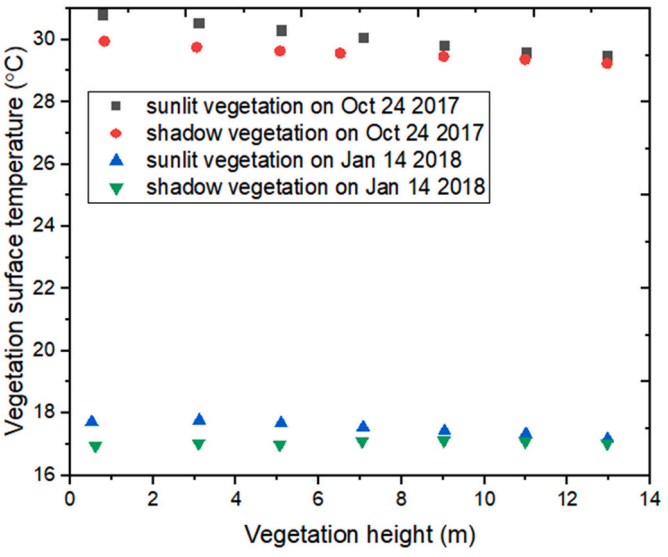

Fig. 18. Vegetation surface temperature vs. vegetation height.

fraction was inconsistent, which might be due to the impact of vegetation shadow on adjacent facets. Neither satellite or airborne thermal data can obtain detailed information on wall surface temperature. As an important component of urban climate, in-situ measurements should be conducted for wall surface temperature research.

Vegetation is an important driver of urban climate (Yu et al., 2020). Thus, numerous studies investigated the cooling effects of vegetation and results showed that these effects depend on the size, shape, composition and configuration of vegetation (Zhou et al., 2011; Zhou et al., 2017). In this study, vegetation surface temperature also changes with the fractional vegetation cover and decreases

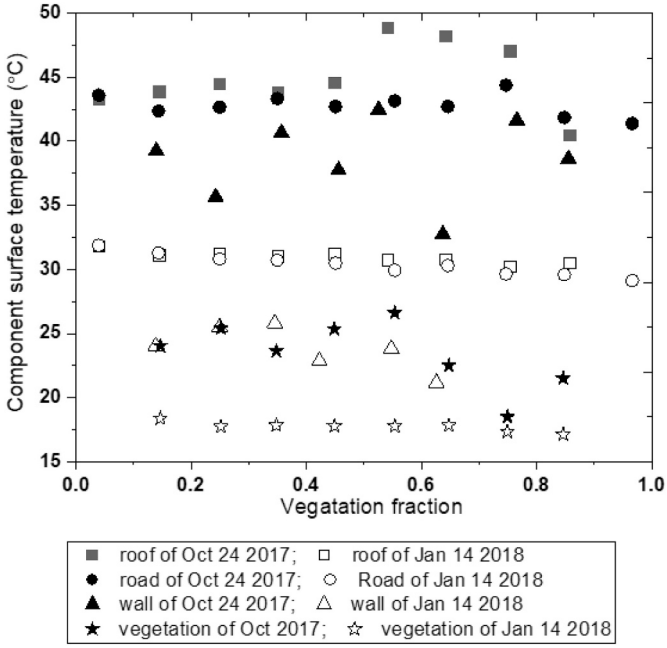

Fig. 19. Component surface temperatures vs. fractional abundance of vegetation in daytime.

Table 8
Regression equations between road / roof day – night temperature difference and fractional abundance of vegetation.

	2017/10/24 daytime	2018/01/14 daytime
Road	$y = -0.9945x + 43.308$ $R^2 = 0.1271$	$y = -3.5775x + 27.685$ $R^2 = 0.7374$
Roof (Fv > 0.5)	$y = -24.917x + 63.564$ $R^2 = 0.7788$	$y = -19.68x + 36.04$ $R^2 = 0.5522$
Wall	$y = -4.5181x + 39.865$ $R^2 = 0.056$	$y = -6.236x + 26.28$ $R^2 = 0.4373$
Vegetation	$y = -2.6483x + 31.703$ $R^2 = 0.9463$	$y = -1.2793x + 18.366$ $R^2 = 0.7165$

with increasing vegetation fraction. Vegetation has very limited impacts on roof surface temperature when a building is higher than vegetation height. On the other hand, T_g decreases with increasing vegetation cover, when vegetation height is higher than road. In general, vegetation only affects the surface temperature of facets which are lower than the vegetation. The study about the impact of tree location and spatial arrangement on outdoor microclimate by Zhao et al. (2018) showed that the shade of trees has significant effects on urban microclimate and thermal comfort. Thus, when vegetation is higher than a facet, the cooling effect of trees is direct and larger than when vegetation is lower than a facet. The temperature of road facets adjacent to vegetation slightly decreases with increasing fractional abundance of vegetation. At the same time, the vegetation surface temperature also decreases with increasing fractional abundance of vegetation. Thus, vegetation cover only affects the surface temperatures of vegetation patches and of facets lower than vegetation height. This may give guidelines relevant to urban design towards better urban climate and also help us understand the satellite thermal infrared observation with low spatial resolution.

Limitations exist in this research. This study only analyzed the geometric effects on facet surface temperatures, while the materials also have large impacts on facet surface temperature, especially for buildings. We used mean values of facet temperatures within bins defined by geometric parameters. This may neglect the variability caused by materials, which we will address in the future. A limited analysis on wall facets was presented in this study. Understanding the role of wall facets is important in urban climate (Hilland and Voogt, 2020), especially in HK with very narrow and tall buildings. The wall structure is also complex. We used the thermal images from different stripes to retrieve the wall surface temperature, but only very few wall facets could be extracted. The wall thermal conditions may be better captured by off-nadir thermal imaging.

Additionally, the building pattern, shape, thickness and material composition also affect the facet surface temperature distribution. Since it is difficult to obtain detailed spatial information on building materials, the building thickness and material composition were not taken into account in this study. The material composition of buildings may affect the urban surface emissivity and then the retrieved surface temperature. For example, some road in the research area is constructed with concrete, and some other road with

asphalt. According to (Kotthaus et al., 2014), the mean emissivity of concrete in urban area is 0.939and the mean emissivity of asphalt is 0.931. This emissivity difference can cause about 0.6 K bias in the retrieved surface temperature. Given the daytime conditions on Oct 242,017, the 0.6 K bias can be neglected compared with the temperature difference caused by geometry, while it cannot be neglected in nighttime. Thus, the material effects on urban surface temperature should be studied carefully based on ground measurement data in the future, especially when using nighttime observations. The building pattern and shape may not have direct relation with building density and height, while they also affect the SVF. Thus, the relationships between facet surface temperature and SVF can show some effects of building pattern and shape.

This study is based on the data collected during four airborne experiments, which were carried out under different weather conditions. Cloud cover was very low, i.e. 14% and 11% on the two days, but we did not obtain observations on cloud cover at exactly the time of flights and on the pattern in cloud cover within the city area.

Net radiation at the surface responds very rapidly to the variability in local cloud cover. Clouds reduce solar irradiance, emit longwave radiation towards the ground surface and absorb the longwave radiation emitted by the ground surface. Changes in net radiation and in the angular distribution of illumination have an impact on the facet surface temperature. In other words, the temporal and spatial variability in cloud conditions might have had an impact on our findings and the effects of urban geometry. Similar comments apply to the variability over a longer period of time in relation with the observed dependence of facet temperatures on urban geometry. On the other hand we combined data acquired during experiments carried out at different time and under different conditions, which gives us some trust in our findings.

Wind speed and direction have likewise large impacts on facet temperatures at locations likely to have strong effects on heat dissipation by convection and, therefore, on facet temperature, especially wall surface temperature (Yang and Li, 2009). Moreover, urban geometry, i.e. building density, building height and SVF (Wang et al., 2018), strongly modifies incoming airflow. We can safely assume that our observations and our relationships by facet type, captured a range of local air flow conditions, thus the relationships between geometric parameters and facet surface temperatures take into account, albeit in an effective sense, the influence of ventilation. On the other hand the complex effects of urban ventilation on urban facet surface temperature, e.g. different effects on street, wall and roof facets, suggest multiple and interesting research questions, which we hope to address in the near future by a combination of in-situ observations, remote sensing and modelling studies.

The thermal camera used in our airborne experiments was calibrated prior to each flight. That notwithstanding, the validation of the HR thermal images against well planned ground measurements would be very beneficial, but unfortunately it was not feasible in our study to deploy an appropriate campaign on in-situ measurements of facet surface temperatures. We expect to augment our investigations on urban climate with systematic ground measurements on urban surface temperature in the near future.

6. Conclusions

This study analyzed the effects of urban geometry on urban land surface temperatures in daytime and nighttime using high spatial resolution airborne thermal images on street/road, rooftop, wall and vegetation facets under different urban conditions. We presented our results on the surface temperature distribution, effects of SVF, building height, building density and vegetation fractional abundance on facet temperatures. Results showed that the geometric parameters have more significant effects on surface temperature of road than roof facets. SVF has more significant effects on T_g than roof surface temperature and higher SVF improves roof heat dissipation; A lower building density is helpful to dissipate street-level excess energy, while higher building density improves roof level heat dissipation. Building density has clearer effects on the surface temperature of road than on roof facets. The vegetation only affects the surface temperatures of vegetation patches and of adjacent facets, if lower than vegetation height. Additionally, the geometric parameters have different effects on component facet temperatures. SVF and building density have obvious effects on the daytime road surface temperature but only SVF has obvious effects on nighttime road surface temperature. As regards daytime roof facet temperature, building height has more significant effects than building density. Neither building density or height have significant effects on nighttime roof surface temperature. Effects of geometric parameters are more significant for sunlit facet temperature than shadow facet temperature.

The effects of urban geometry on the surface temperature of each facet type, i.e. road, roof, wall and vegetation, have been studied thoroughly in the past, but studies based on HR thermal images, are very scarce to our best knowledge. Different facet types play different roles in the urban thermal exchange. Thus, it is necessary to understand how the urban geometry affects the surface temperature of different facet types. This study is based on HR observations of facet surface temperature and tries to document how the response of different types of urban facets to radiative and convective forcing is modulated by urban geometry, i.e. by the conditions in the vicinity of the observed targets. We regard this as our main innovative contribution. The high-resolution data sets used in our study will open up several avenues for further research, particularly on the role of vegetation in urban climate.

This research can provide suggestions for urban planning and designing to understand the urban thermal environment and improve the sustainability of the cities in the near future.

Declaration of Competing Interest

The authors declare no conflict of interest.

Acknowledgement

This work was supported by Grants by National Natural Science Foundation of China (41901283, 61976234, 42071394), Guangdong Provincial Natural Science Foundation (2021A1515012567, 2018B030312004), and Major Projects of High Resolution Earth Observation (Grant No. 30-H30C01-9004-19/21). The authors thank the Hong Kong Planning Department, Hong Kong Lands Department, the Hong Kong Civil Engineering and Development Department, the Hong Kong Observatory and the Hong Kong Government Flying Service for the planning, building GIS, weather and climate, and airborne Lidar data. Massimo Menenti acknowledges the support of grant P10-TIC-6114 by the Junta de Andalucía and the MOST High Level Foreign Expert program (Grant nr. GL20200161002). Man Sing Wong thanks the funding support from a grant by the General Research Fund (Grant no. 15602619) from the Hong Kong Research Grants Council. Dr. Qunshan Zhao has received UK ESRC's on-going support for the Urban Big Data Centre (UBDC) [ES/L011921/1 and ES/S007105/1]. We would also want to thank the anonymous reviewers for their insightful comments and suggestions on an earlier version of this manuscript.

References

Ali-Toudert, F., Mayer, H., 2006. Numerical study on the effects of aspect ratio and orientation of an urban street canyon on outdoor thermal comfort in hot and dry climate. Build. Environ. 41 (2), 94–108.
Baldridge, A., Hook, S., Grove, C., Rivera, G., 2009. The ASTER spectral library version 2.0. Remote Sens. Environ. 113 (4), 711–715.
Chen, X.-L., Zhao, H.-M., Li, P.-X., Yin, Z.-Y., 2006. Remote sensing image-based analysis of the relationship between urban heat island and land use/cover changes. Remote Sens. Environ. 104 (2), 133–146.
Franck, U., et al., 2013. Heat stress in urban areas: indoor and outdoor temperatures in different urban structure types and subjectively reported well-being during a heat wave in the city of Leipzig. Meteorol. Z. 22 (2), 167–177.
Goldberg, V., Kurbjuhn, C., Bernhofer, C., 2013. How Relevant Is Urban Planning for the Thermal Comfort of Pedestrians? Numerical Case Studies in Two Districts of the City of Dresden (Saxony/Germany).
Harman, I., Best, M., Belcher, S., 2004. Radiative exchange in an urban street canyon. Bound.-Layer Meteorol. 110 (2), 301–316.
Henon, A., Lagouarde, J., Mestayer, P., Groleau, D., 2009. High resolution surface temperature and urban thermal anisotropy simulations: validation against airborne remote sensing TIR data over Toulouse city (France). In: 8th AMS Symp. on Urban Environment, Phoenix AZ, Poster Session.
Hilland, R.V.J., Voogt, J.A., 2020. The effect of sub-facet scale surface structure on wall brightness temperatures at multiple scales. Theor. Appl. Climatol. 140, 767–785. https://doi.org/10.1007/s00704-020-03094-7.
Hou, H., Estoque, R., 2020. Detecting cooling effect of landscape from composition and configuration: an urban heat island study on Hangzhou. Urban For. Urban Green. 126719.
Hu, L., Brunsell, N.A., 2013. The impact of temporal aggregation of land surface temperature data for surface urban heat island (SUHI) monitoring. Remote Sens. Environ. 134, 162–174.
Huang, X., Wang, Y., 2019. Investigating the effects of 3D urban morphology on the surface urban heat island effect in urban functional zones by using high-resolution remote sensing data: a case study of Wuhan, Central China. ISPRS J. Photogramm. Remote Sens. 152, 119–131.
Kanda, M., et al., 2005. A simple energy balance model for regular building arrays. Bound.-Layer Meteorol. 116 (3), 423–443.
Kastendeuch, P.P., Najjar, G., 2009. Simulation and validation of radiative transfers in urbanised areas. Sol. Energy 83 (3), 333–341.
Kondo, A., Ueno, M., Kaga, A., Yamaguchi, K., 2001. The influence of urban canopy configuration on urban albedo. Bound.-Layer Meteorol. 100 (2), 225–242.
Kotthaus, S., Smith, T.E.L., Wooster, M.J., Grimmond, C.S.B., 2014. Derivation of an urban materials spectral library through emittance and reflectance spectroscopy. ISPRS J. Photogramm. Remote Sens. 94 (0), 194–212.
Krayenhoff, E.S., Voogt, J., 2007. A microscale three-dimensional urban energy balance model for studying surface temperatures. Bound.-Layer Meteorol. 123 (3), 433–461.
Lagouarde, J.P., Irvine, M., 2008. Directional anisotropy in thermal infrared measurements over Toulouse city centre during the CAPITOUL measurement campaigns: first results. Meteorog. Atmos. Phys. 102 (3–4), 173–185.
Lagouarde, J.-P., et al., 2004. Airborne experimental measurements of the angular variations in surface temperature over urban areas: case study of Marseille (France). Remote Sens. Environ. 93 (4), 443–462.
Lagouarde, J.P., et al., 2010. Modelling daytime thermal infrared directional anisotropy over Toulouse city centre. Remote Sens. Environ. 114 (1), 87–105.
Lagouarde, J.-P., et al., 2012. Experimental characterization and modelling of the nighttime directional anisotropy of thermal infrared measurements over an urban area: case study of Toulouse (France). Remote Sens. Environ. 117, 19–33.
Lai, A., So, A.C., Ng, S., Jonas, D., 2012. The territory-wide airborne light detection and ranging survey for the Hong Kong special administrative region. In: The 33RD Asian Conference on Remote Sensing, pp. 26–30.
Li, J., et al., 2011. Impacts of landscape structure on surface urban heat islands: a case study of Shanghai, China. Remote Sens. Environ. 115 (12), 3249–3263.
Logan, T.M., Zaitchik, B., Guikema, S., Nisbet, A., 2020. Night and day: the influence and relative importance of urban characteristics on remotely sensed land surface temperature. Remote Sens. Environ. 247, 111861.
Menenti, M., et al., 2001. Estimation of soil and vegetation temperatures with multiangular thermal infrared observations: IMGRASS, HEIFE, and SGP 1997 experiments. J. Geophys. Res. 106 (D11), 11997–12010.
Morrison, W., et al., 2018. A novel method to obtain three-dimensional urban surface temperature from ground-based thermography. Remote Sens. Environ. 215, 268–283.
Ng, E., Chen, L., Wang, Y., Yuan, C., 2012. A study on the cooling effects of greening in a high-density city: an experience from Hong Kong. Build. Environ. 47, 256–271.
Oke, T., 1988. The urban energy balance. Prog. Phys. Geogr. 12 (4), 471–508.
Oke, T.R., Spronken-Smith, R.A., Jáuregui, E., Grimmond, C.S.B., 1999. The energy balance of central Mexico City during the dry season. Atmos. Environ. 33 (24–25), 3919–3930.
Peng, J., et al., 2020. A wavelet coherence approach to prioritizing influencing factors of land surface temperature and associated research scales. Remote Sens. Environ. 246, 111866.
United Nations, 16 May 2018. https://www.un.org/development/desa/en/news/population/2018-revision-of-world-urbanization-prospects.html.
Voogt, J.A., Oke, T.R., 2003. Thermal remote sensing of urban climates. Remote Sens. Environ. 86 (3), 370–384.
Wang, Z.-H., 2014. Monte Carlo simulations of radiative heat exchange in a street canyon with trees. Sol. Energy 110, 704–713.
Wang, D., Chen, Y., Zhan, W., 2018. A geometric model to simulate thermal anisotropy over a sparse urban surface (GUTA-sparse). Remote Sens. Environ. 209, 263–274.
Wang, D., et al., 2020. An advanced geometric model to simulate thermal anisotropy time-series for simplified urban neighborhoods (GUTA-T). Remote Sens. Environ. 237, 111547.
Weng, Q., 2009. Thermal infrared remote sensing for urban climate and environmental studies: methods, applications, and trends. ISPRS J. Photogramm. Remote Sens. 64 (4), 335–344.

Weng, Q., Lu, D., Schubring, J., 2004. Estimation of land surface temperature–vegetation abundance relationship for urban heat island studies. Remote Sens. Environ. 89 (4), 467–483.
Wentz, E.A., et al., 2018. Six fundamental aspects for conceptualizing multidimensional urban form: a spatial mapping perspective. Landsc. Urban Plan. 179, 55–62.
Wetherley, E.B., McFadden, J.P., Roberts, D.A., 2018. Megacity-scale analysis of urban vegetation temperatures. Remote Sens. Environ. 213, 18–33.
Xu, W., Wooster, M., Grimmond, C., 2008. Modelling of urban sensible heat flux at multiple spatial scales: a demonstration using airborne hyperspectral imagery of Shanghai and a temperature–emissivity separation approach. Remote Sens. Environ. 112 (9), 3493–3510.
Yaghoobian, N., Kleissl, J., Krayenhoff, E.S., 2010. Modeling the thermal effects of artificial turf on the urban environment. J. Appl. Meteorol. Climatol. 49 (3), 332–345.
Yang, X., Li, Y., 2013. Development of a three-dimensional urban energy model for predicting and understanding surface temperature distribution. Bound.-Layer Meteorol. 149 (2), 303–321.
Yang, Lina, Li, Yuguo, 2009. City ventilation of Hong Kong at no-wind conditions. Atmos. Environ. 43, 3111–3121. https://doi.org/10.1016/j.atmosenv.2009.02.062.
Yang, X., Li, Y., 2015. The impact of building density and building height heterogeneity on average urban albedo and street surface temperature. Build. Environ. 90 (0), 146–156.
Yang, J., et al., 2016. Development of an improved urban emissivity model based on sky view factor for retrieving effective emissivity and surface temperature over urban areas. ISPRS J. Photogramm. Remote Sens. 122, 30–40.
Yang, J., et al., 2020. A semi-empirical method for estimating complete surface temperature from radiometric surface temperature, a study in Hong Kong city. Remote Sens. Environ. 237, 111540.
Yang, J., et al., 2021. Assessing the impact of urban geometry on surface urban heat island using complete and nadir temperatures. Int. J. Climatol. 41 (S1), E3219–E3238.
Yu, K., et al., 2019. Study of the seasonal effect of building shadows on urban land surface temperatures based on remote sensing data. Remote Sens. 11 (5), 497.
Yu, Z., et al., 2020. Critical review on the cooling effect of urban blue-green space: a threshold-size perspective. Urban For. Urban Green. 49, 126630.
Yuan, F., Bauer, M.E., 2007. Comparison of impervious surface area and normalized difference vegetation index as indicators of surface urban heat island effects in Landsat imagery. Remote Sens. Environ. 106 (3), 375–386.
Zhan, W., et al., 2012. Assessment of thermal anisotropy on remote estimation of urban thermal inertia. Remote Sens. Environ. 123, 12–24.
Zhao, Q., Wentz, E.A., 2016. A MODIS/ASTER airborne simulator (master) imagery for urban Heat Island research. Data 1 (1), 7.
Zhao, Q., Myint, S., Wentz, E., Fan, C., 2015. Rooftop surface temperature analysis in an urban residential environment. Remote Sens. 7, 12135–12159.
Zhao, Q., Sailor, D.J., Wentz, E.A., 2018. Impact of tree locations and arrangements on outdoor microclimates and human thermal comfort in an urban residential environment. Urban For. Urban Green. 32, 81–91.
Zhou, J., Chen, Y., Wang, J., Zhan, W., 2011. Maximum nighttime urban heat island (UHI) intensity simulation by integrating remotely sensed data and meteorological observations. IEEE J. Select. Topics Appl. Earth Observ. Remote Sens. 4 (1), 138–146.
Zhou, W., Wang, J., Cadenasso, M., 2017. Effects of the spatial configuration of trees on urban heat mitigation: a comparative study. Remote Sens. Environ. 195.